Electronic Supplementary Material (ESI) for New Journal of Chemistry.

Supporting information

$CuCo_2O_4$ Nanoparticles Wrapped in a rGO Aerogel Composite as an Anode for a Fast and Stable Li-ion Capacitor with ultra-high specific energy

Muhammad Sajjad*[a], Muhammad Sufyan Javed[b], Muhammad Imran[c], Zhiyu Mao

[a]Yunnan Key Laboratory for Micro/Nano Materials & Technology, National Center for International Research on Photoelectric and Energy Materials, School of Materials and Energy, Yunnan University, Kunming 650091, P. R China

[b]School of Physical Science and Technology, Lanzhou University, Lanzhou 730000, China

[c]Department of Chemistry, Faculty of Science, King Khalid University, Abha 61413, Saudi Arabia

[d]*College of Chemistry and Life Sciences, Zhejiang Normal University, Jinhua, 321004, P. R China*

**Corresponding author: sajjadfisica@gmail.com and zhymao@zjnu.edu.cn*

1. Calculations

The formulas for calculating energy and power densities are the following:

$$\mathbf{C_{anode} \times \Delta V_{anode} \times m_{anode} = C_{cathode} \times \Delta V_{cathode} \times m_{cathode}} \quad \text{… (S-1)}$$

$$C = \frac{I \times \Delta t}{m \times \Delta V} \quad \text{… (S-2)}$$

$$E = \frac{C_s \times \Delta V^2}{2} \quad \text{... (S-3)}$$

$$P = \frac{\mathbf{E}}{\mathbf{\Delta t}} \quad \text{… (S-4)}$$

C_s is the specific capacitance, m is the electrode's mass, ΔV is the potential range, and Δt is the discharge time.

Table S1. The structural parameters of the samples.

Sample	BET surface area (m^2 g^{-1})	Pore diameter (nm)
$CuCo_2O_4$	10	42
$CuCo_2O_4$/rGO composite	43	7.6

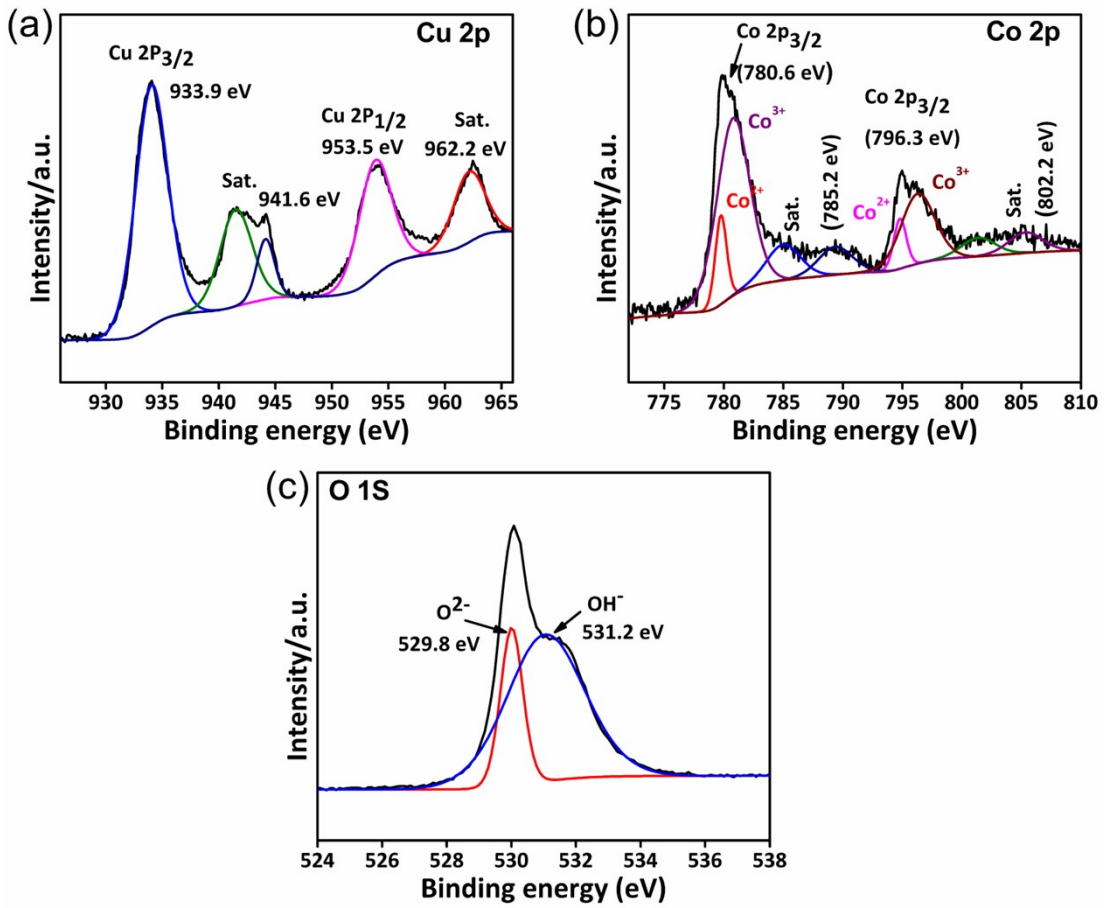

Figure S1. High-resolution XPS spectra of Cu (a) high-resolution XPS spectra of Cu 2p, (b) Co 2p, (c) O 1s, respectively, of $CuCo_2O_4$ sample.

1. Rate performance of LIBs

To demonstrate the performance of $CuCo_2O_4$/rGO composite for LIBs, a coin-type battery was assembled and tested in a potential frame of 0 to 3.0 V. The electrochemical performance was investigated by CV, GCD, and EIS measurements. The GCD curves of $CuCo_2O_4$ nanoparticles and $CuCo_2O_4$/rGO composite electrodes at the current density of 0.1 A g^{-1} are shown in **Fig. S2a, b**. In **Fig. S2a**, two weak declined plateaus are observed between 2.0 V and 1.2 V during the 1st discharge cycle, corresponding to the formation of the solid-electrolyte-interphase (SEI) layer [1, 2] and Li_2O[3]. The first specific discharge and charge capacities are 534.3 and 507.8 mAh g^{-1}, respectively. During the cycling from the 1st to the 3rd, the charge and discharge specific

capacities remain unchanged, and the curve coincidence is high, reflecting good capacity maintenance of the $CuCo_2O_4$ electrode. Likewise, the $CuCo_2O_4$/rGO composite electrode's GCD profile shows a weak plateau between 0.9 and 1.33 V, corresponding to the SEI layer as depicted in **Fig. S2b** [4]. Furthermore, $CuCo_2O_4$/rGO composite electrode achieved almost complete retention of coulombic efficiency together with an initial specific discharge capacity of 1285 mAh g^{-1}. The obtained specific capacity is much higher than its theoretical one (874 mAh g^{-1}), which may be attributed to the formation of SEI film, the mesoporous nanostructure, and synergistic effect of rGO aerogel [5]. **Fig. S2c** shows the cycling performance, corresponding to the charging-discharging curves, of $CuCo_2O_4$ and $CuCo_2O_4$/rGO composite electrode at 0.5 A g^{-1}. The reversible specific capacities of $CuCo_2O_4$/rGO and $CuCo_2O_4$ composite electrodes are 1285 mAh g^{-1} and 760 mAh g^{-1}, respectively, and almost complete retention of discharge efficiency was achieved over 300 loops, indicating an outstanding cycling performance. Additionally, the capacity increases with increasing cycle number, which may be due to activation of the active material, owing to the increased electrode/electrolyte interface area.[6] Similarly, at the current density of 0.1 A g^{-1}, both samples display a similar cycling stability trend without significant degradation even after 60 cycles, demonstrating their good stability **(Fig. S2d)**. The low first coulombic efficiency of ~76% is due to the irreversible reactions at the electrode in the first cycle. In the subsequent 100 to 300 cycles, a continuous capacity increase occurs because of the reversible formation and decomposition of a polymeric gel-like film during the electrochemical activation process[7], probably originating from the kinetically activated electrolyte degradation, and the generation of more defects and active sites for lithium-ion storage.[8, 9] During the cycling, both electrodes' reversible specific capacities remain stable without obvious decline tendency, exhibiting extraordinary stability and reversibility. The synergistic effect between the $CuCo_2O_4$ nanoparticle

and the rGO aerogel network could account for the excellent performance of the electrode material, where the nanoscale particle size of $CuCo_2O_4$ enriches the active sites while the rGO aerogel conductive network makes them more accessible for the storage of Li^+. The rate performance is the essential parameter of any material for the practical relevance that defines commercialization's suitability. Herein, $CuCo_2O_4$ nanoparticles and $CuCo_2O_4$/rGO composite were further evaluated at various current densities of 0.1, 0.2, 0.5, 1, and 2 A g^{-1} to test their rate performance and the results are depicted in **Fig. S2e**. It was revealed that the $CuCo_2O_4$/rGO exhibited much higher (compared to $CuCo_2O_4$) specific capacities of 586, 465, 336, 264, and 207 mAh g^{-1} at 0.1, 0.2, 0.5, 1, and 2 A g^{-1}, respectively. When the current density reverses back to 0.1 A g^{-1}, the specific capacity is still high (578 mAh g^{-1}). These excellent results signify the excellent electrochemical stability and cyclic reversibility of the $CuCo_2O_4$/rGO unique structures.

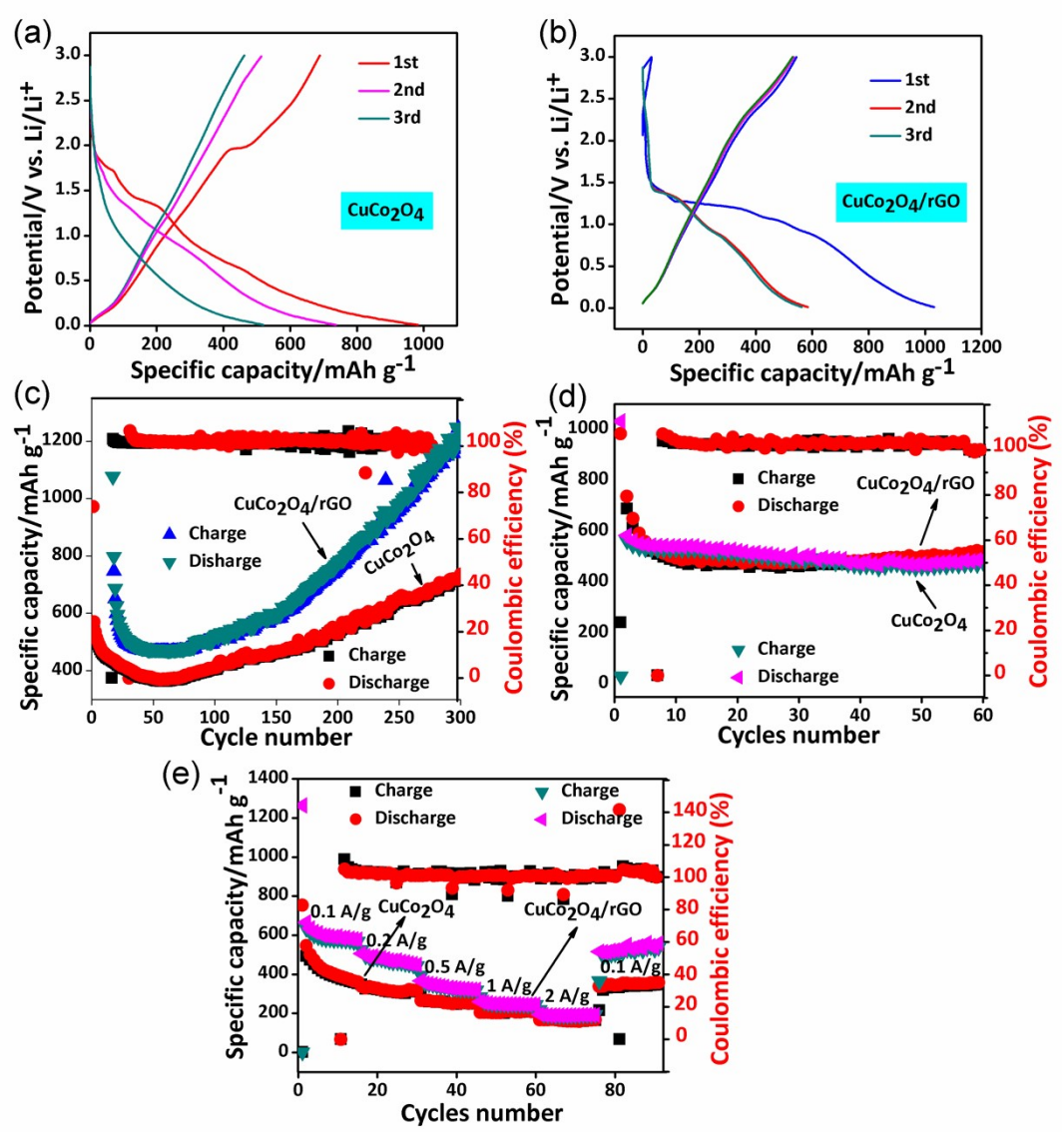

Figure S2. Electrochemical performances of LIBs, (a, b) Charge-discharge curves of $CuCo_2O_4$, and $CuCo_2O_4$/rGO electrodes, respectively, (c) cycling performance at 0.5 A g^{-1}, (d) cycling performance at 0.1 A g^{-1}, and (e) the rate performance of $CuCo_2O_4$, and $CuCo_2O_4$/rGO electrodes.

In the cause of certifying the rapid kinetics of $CuCo_2O_4$/rGO composite. We calculated and investigated $CuCo_2O_4$/rGO composite and $CuCo_2O_4$ nanoparticles' control processes and qualitatively analyzed their capacitive contribution characteristics. The current response in a CV

curve is generally classified into three categories. In a battery system, the diffusion control volume response and the capacitive surface response generally constitute a Faraday current response. This restriction process can be expressed by the following formula[10]:

$$i = a \times v^b \qquad \ldots \text{(S-6)}$$

where v is the scan rate, and a is the constant. A b value of 0.5 indicates a half-infinite linear diffusion-controlled. The b value of 1 indicates a current that is not limited by diffusion but controlled by a surface redox reaction. **Fig. S3a, b** shows a b value for $CuCo_2O_4$, and $CuCo_2O_4$/rGO, respectively, obtained from the scan speed and peak current corresponding to the unique redox peak. It can be known that the b value of the $CuCo_2O_4$/rGO composite electrode is 0.99 and the $CuCo_2O_4$ is only 0.53, which indicates that the $CuCo_2O_4$/rGO composite electrode system has an ultra-fast kinetic process because it is not subject to diffusion control[11]. This process is mainly due to the rGO conductive network's addition, making the $CuCo_2O_4$ nanoparticles have a unique transmission capacity in Li^+ insertion-extraction for charge-discharge.

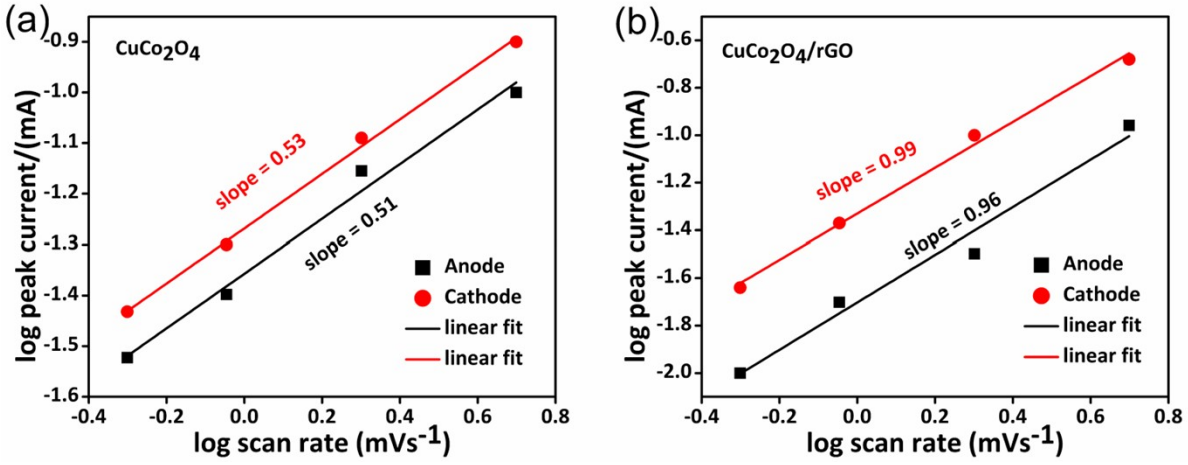

Figure S3. Dynamics performance of LIBs: (a, b) The b value of $CuCo_2O_4$, and $CuCo_2O_4$/rGO, respectively.

Fig. S4 presents the Bode plots showed the relationship between phase angle and frequency. The frequency *f* describes the maximum frequency at the phase angle of 45º, where the capacitive behavior is leading. Obviously, a bit higher phase angle of (-80º) for $CuCo_2O_4$/rGO was observed compared to pristine $CuCo_2O_4$, indicating the excellent performance of the composite electrode material with fast ion transport efficiency. The typical Nyquist plots are usually used to describe the specific process in the electrode material of ion and electron transport, including the intrinsic impedance R_s of the electrode material in contact with the electrode and the electrode/electrolyte interface of the surface film R_{sf} and the charge transfer resistance Rct. The influence factors of impedance mainly include the path and channel of Li^+ transmission and electrons' conductivity. **Fig. S4b** shows the transmission capacity of ions and electrons in a fresh battery. It can be observed that $CuCo_2O_4$/rGO composite have minimal intrinsic impedance and charge transfer impedance compared to $CuCo_2O_4$ nanoparticles **(Table. S2)**, which can be attributed to the addition of rGO conductive networks to enable electrons to be fast on conductive networks as depicted in the enlarged view in **Fig. S4c**.

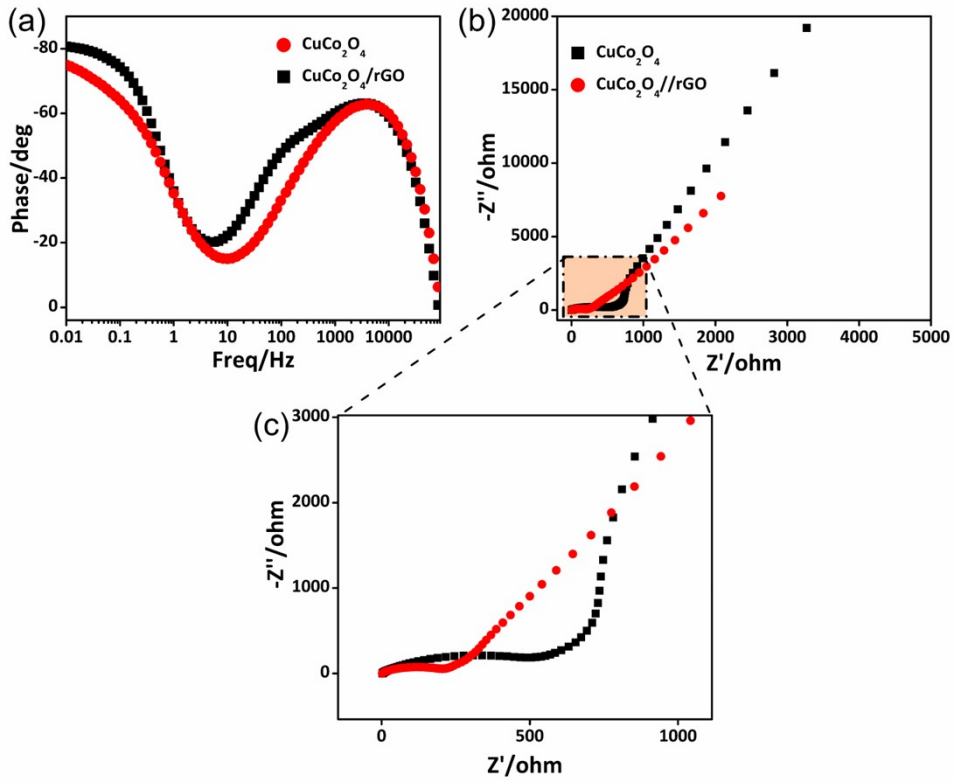

Figure S4. (a) Bode plots of $CuCo_2O_4$ and $CuCo_2O_4$/rGO, (b) Nyquist plots of $CuCo_2O_4$ and $CuCo_2O_4$/rGO composite, (c) the corresponding zoom-in view of the impedance plots.

Table S2. Summary of simulation results (by Z-View software) from EIS spectra.

Sample	**R_s(Ω)**	**R_{ct} + sf(Ω)**
$CuCo_2O_4$/rGO	6.25	75.4
$CuCo_2O_4$	15.48	726

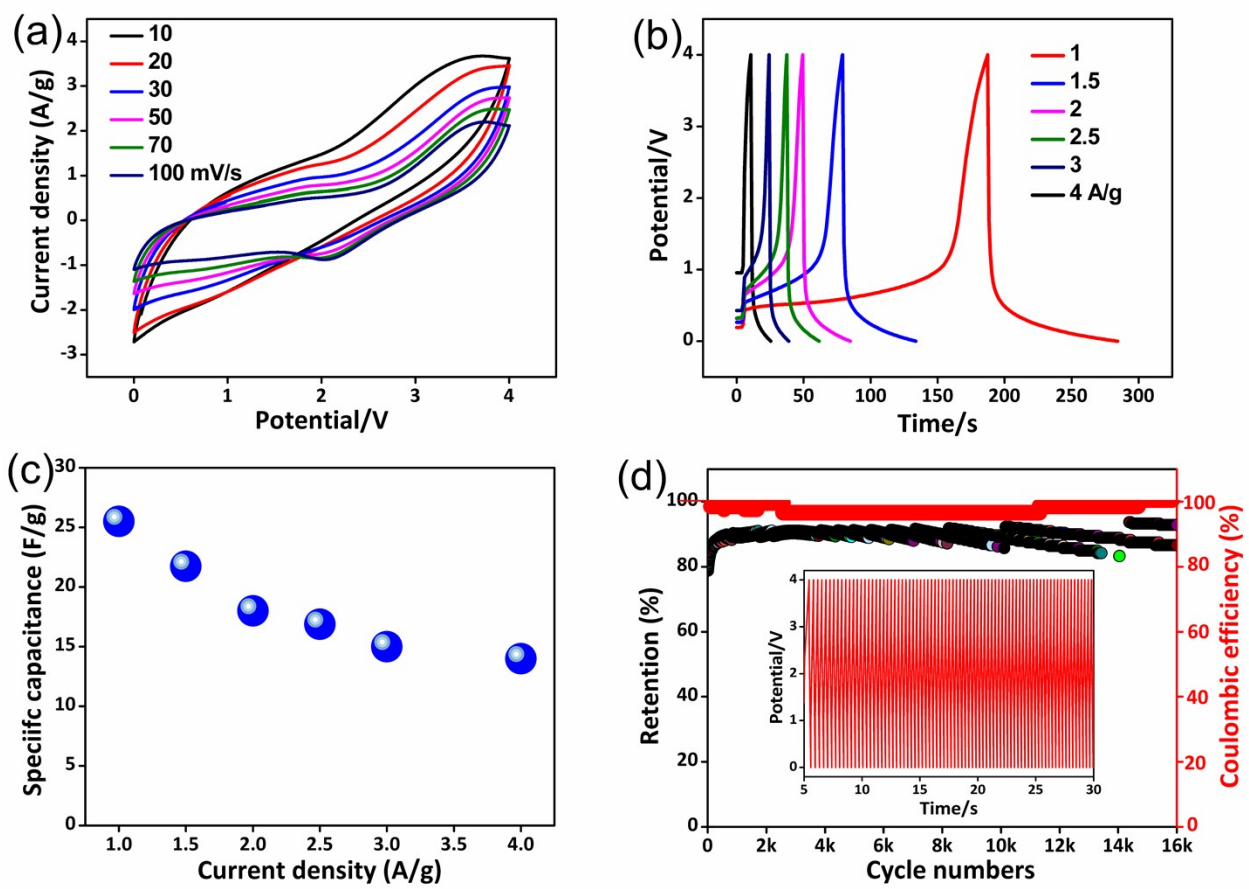

Figure S5. CV curves of $CuCo_2O_4$//AC LIC at various scan rates, (b) GCD profile at different current densities, (c) cycling stability test (the inset shows the last nine cycles).

References

1. Huang, X.; Zhang, Z.; Li, H.; Zhao, Y.; Wang, H.; Ma, T., Novel fabrication of Ni3S2/MnS composite as high performance supercapacitor electrode. *Journal of Alloys Compounds* **2017,** *722*, 662-668.
2. Han, D.; Hu, H.; Liu, B.; Song, G.; Yan, H.; Di, J., CuCo2O4 nanoparticles encapsulated by onion-like carbon layers: a promising solution for high-performance lithium ion battery. *Ceramics International* **2016,** *42* (10), 12460-12466.
3. Deng, Y.; Zhang, Q.; Tang, S.; Zhang, L.; Deng, S.; Shi, Z.; Chen, G., One-pot synthesis of ZnFe2O4/C hollow spheres as superior anode materials for lithium ion batteries. *Chemical Communications* **2011,** *47* (24), 6828-6830.
4. Niu, J. L.; Zeng, C. H.; Peng, H. J.; Lin, X. M.; Sathishkumar, P.; Cai, Y. P., Formation of N-Doped Carbon-Coated ZnO/ZnCo2O4/CuCo2O4 Derived from a Polymetallic Metal–Organic Framework: Toward High-Rate and Long-Cycle-Life Lithium Storage. *Small* **2017,** *13* (47), 1702150.
5. Cai, S.; Wang, G.; Jiang, M.; Wang, H., Template-free fabrication of porous CuCo 2 O 4 hollow spheres and their application in lithium ion batteries. *Journal of Solid State Electrochemistry* **2017,** *21* (4), 1129-1136.

6. Sun, Y.; Hu, X.; Luo, W.; Xia, F.; Huang, Y., Reconstruction of Conformal Nanoscale MnO on Graphene as a High-Capacity and Long-Life Anode Material for Lithium Ion Batteries. *Advanced Functional Materials* **2013,** *23* (19), 2436-2444.
7. Ma, J.; Wang, H.; Yang, X.; Chai, Y.; Yuan, R., Porous carbon-coated CuCo 2 O 4 concave polyhedrons derived from metal–organic frameworks as anodes for lithium-ion batteries. *Journal of Materials Chemistry A* **2015,** *3* (22), 12038-12043.
8. Wei, W.; Yang, S.; Zhou, H.; Lieberwirth, I.; Feng, X.; Müllen, K., 3D Graphene Foams Cross-linked with Pre-encapsulated Fe3O4 Nanospheres for Enhanced Lithium Storage. *Advanced Materials* **2013,** *25* (21), 2909-2914.
9. Chang, K.; Geng, D.; Li, X.; Yang, J.; Tang, Y.; Cai, M.; Li, R.; Sun, X., Ultrathin MoS2/Nitrogen-Doped Graphene Nanosheets with Highly Reversible Lithium Storage. *Advanced Energy Materials* **2013,** *3* (7), 839-844.
10. Sajjad, M.; Jiang, Y.; Guan, L.; Chen, X.; Iqbal, A.; Zhang, S.; Ren, Y.; Zhou, X.; Liu, Z., NiCo2S4 nanosheet grafted SiO2@ C core-shelled spheres as a novel electrode for high performance supercapacitors. *Nanotechnology* **2019,** *31* (4), 045403.
11. Li, Q.; Yin, L.; Li, Z.; Wang, X.; Qi, Y.; Ma, J., Copper doped hollow structured manganese oxide mesocrystals with controlled phase structure and morphology as anode materials for lithium ion battery with improved electrochemical performance. *ACS Appl. Mater. Interfaces* **2013,** *5* (21), 10975-10984.